# Proton transfers are key elementary steps in ethylene polymerization on isolated chromium(III) silicates

Murielle F. Delley[a], Francisco Núñez-Zarur[a], Matthew P. Conley[a], Aleix Comas-Vives[a], Georges Siddiqi[a], Sébastien Norsic[b], Vincent Monteil[b], Olga V. Safonova[c], and Christophe Copéret[a,1]

[a]Department of Chemistry and Applied Biosciences, Eidgenössische Technische Hochschule Zürich, CH-8093 Zürich, Switzerland; [b]Laboratoire de Chimie Catalyse Polymères et Procédés, Unité Mixte de Recherche 5265, Université de Lyon, 69616 Villeurbanne, France; and [c]General Energy Research Department, Paul Scherrer Institute, CH-5232 Villigen, Switzerland

Edited* by John Bercaw, California Institute of Technology, Pasadena, CA, and approved June 13, 2014 (received for review March 21, 2014)

**Mononuclear Cr(III) surface sites were synthesized from grafting [Cr(OSi(O$^t$Bu)$_3$)$_3$(tetrahydrofurano)$_2$] on silica partially dehydroxylated at 700 °C, followed by a thermal treatment under vacuum, and characterized by infrared, ultraviolet-visible, electron paramagnetic resonance (EPR), and X-ray absorption spectroscopy (XAS). These sites are highly active in ethylene polymerization to yield polyethylene with a broad molecular weight distribution, similar to that typically obtained from the Phillips catalyst. CO binding, EPR spectroscopy, and poisoning studies indicate that two different types of Cr(III) sites are present on the surface, one of which is active in polymerization. Density functional theory (DFT) calculations using cluster models show that active sites are tricoordinated Cr(III) centers and that the presence of an additional siloxane bridge coordinated to Cr leads to inactive species. From IR spectroscopy and DFT calculations, these tricoordinated Cr(III) sites initiate and regulate the polymer chain length via unique proton transfer steps in polymerization catalysis.**

C–H activation | heterogeneous catalysis

Almost half of the world's high-density polyethylene is produced by the Phillips catalyst, a silica-supported chromium oxide ($CrO_x/SiO_2$) (1). This catalyst is prepared by incipient wetness impregnation of a chromium salt on silica, followed by high temperature calcination. Contacting this material with ethylene forms the active reduced species in situ that polymerizes ethylene. The Phillips catalyst is active in the absence of activators that are typically required for polymerization catalysts (2). Despite 50 y of research, the catalytically active site and the initiation mechanism, particularly the formation of the first Cr–C bond, remain controversial. Numerous spectroscopic techniques [infrared (IR), ultraviolet-visible (UV-Vis), electron paramagnetic resonance (EPR), X-ray absorption spectroscopy (XAS), etc.] established that the Phillips catalyst contains a complex mixture of surface Cr species, of which only ∼10% are active in polymerization (3, 4). The low number of active sites is one of the main limiting factors in using spectroscopic methods to study this material because the spectroscopic signature mainly belongs to inactive species.

Previous molecular approaches to determine the Phillips catalyst ethylene polymerization mechanism focused on systems containing preformed Cr–C bonds (5–7). We recently reported the preparation of well-defined silica-supported Cr(II) and Cr(III) dinuclear sites (8), where Cr(III) species are active polymerization sites, in contrast to Cr(II), which is consistent with extensive research on homogeneous chromium complexes (9–11). We proposed that these well-defined Cr(III) silicates initiate polymerization by the heterolytic cleavage of a C–H bond of ethylene on a Cr–O bond to form a Cr–vinyl species that is capable of inserting ethylene by a Cossee–Arlman mechanism (8). However, extensive studies on Phillips catalyst invoke mononuclear polymerization sites (12–18). Furthermore, direct evidence of the active site structure and the polymerization mechanism is critically needed. Here we investigate the preparation and the detailed characterization of isolated Cr(III) sites supported on silica, prepared by grafting [Cr$^{III}$(OSi(O$^t$Bu)$_3$)$_3$(tetrahydrofurano; THF)$_2$] (19) on dehydroxylated silica and a subsequent thermal treatment under vacuum. These isolated Cr(III) sites are highly active in ethylene polymerization in the absence of coactivator. Computational investigations in combination with IR spectroscopy indicate that polymerization occurs on tricoordinate Cr(III) sites and involves two key proton transfer steps: (*i*) formation of the first Cr–C bond through the C–H activation of ethylene across a Cr–O bond and (*ii*) termination by the microreverse of the initiation step while chain growth occurs by classical Cossee–Arlman insertion polymerization (20, 21).

## Results and Discussion

**Catalyst Preparation and Characterization.** Mononuclear Cr(III) sites were prepared as shown in Fig. 1*A*. Silica partially dehydroxylated at 700 °C ($SiO_{2-700}$, 0.26 mmol SiOH/g) reacts with a bluish green benzene solution of [Cr(OSi(O$^t$Bu)$_3$)$_3$(THF)$_2$] (**1**) (19) to form a light blue solid [(≡SiO)Cr(OSi(O$^t$Bu)$_3$)$_2$(THF)] (**2**) and 0.10 mmol of ($^t$BuO)$_3$SiOH. Elemental analysis of **2** gives 0.85 wt% Cr, 4.92 wt% C, and 0.91 wt% H that corresponds to 0.16 mmol Cr/g and 25 ± 1 C/Cr close to the expected value (28 C/Cr) for a monografted species. The IR spectrum of **2** contains a broad band at 3,705 cm$^{-1}$ from silanols interacting with the organic moieties of the grafted species and C–H bands at 2,980–2,880 and 1,480–1,370 cm$^{-1}$ that are consistent with the presence of –(OSi(O$^t$Bu)$_3$)$_3$ and THF (Fig. S1*A*).

Thermal treatment of **2** under high vacuum ($10^{-5}$ mbar) at elevated temperatures yields the light blue solid [(≡SiO)$_3$Cr] (**3**) that lacks C-H bands and contains new SiOH bands in the IR spectrum (Fig. S1*A*). Quantification of the volatile fraction gives 6.6 equivalents of isobutene, 0.2 equivalents of $^t$BuOH, and 1 equivalent

### Significance

**The Phillips catalyst—$CrO_x/SiO_2$—produces 40–50% of global high-density polyethylene, yet several fundamental mechanistic controversies surround this catalyst. What is the oxidation state and nuclearity of the active Cr sites? How is the first Cr–C bond formed? How does the polymer propagate and regulate its molecular weight? Here we show through combined experimental (infrared, ultraviolet-visible, X-ray near edge absorption spectroscopy, and extended X-ray absorption fine structures) and density functional theory modeling approaches that mononuclear tricoordinate Cr(III) sites immobilized on silica polymerize ethylene by the classical Cossee–Arlman mechanism. Initiation (C–H bond activation) and polymer molecular weight regulation (the microreverse of C–H activation) are controlled by proton transfer steps.**

Author contributions: M.F.D., F.N.-Z., M.P.C., A.C.-V., and C.C. designed research; M.F.D., F.N.-Z., G.S., and S.N. performed research; M.F.D., F.N.-Z., M.P.C., A.C.-V., S.N., V.M., O.V.S., and C.C. analyzed data; and M.F.D., F.N.-Z., M.P.C., and C.C. wrote the paper.

The authors declare no conflict of interest.

*This Direct Submission article had a prearranged editor.

See Commentary on page 11578.

[1]To whom correspondence should be addressed. Email: ccoperet@ethz.ch.

This article contains supporting information online at www.pnas.org/lookup/suppl/doi:10.1073/pnas.1405314111/-/DCSupplemental.

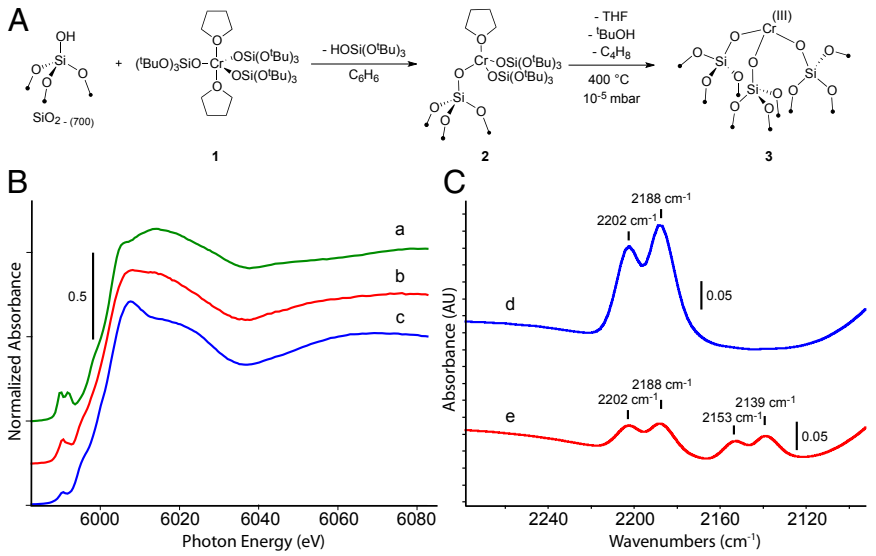


**Fig. 1.** (*A*) Grafting of $[Cr(OSi(O^tBu)_3)_3(THF)_2]$ (**1**) on $SiO_{2-700}$ giving $[(\equiv SiO)Cr(OSi(O^tBu)_3)_2(THF)]$ (**2**) and thermal treatment of **2** yielding $[(\equiv SiO)_3Cr]$ (**3**). (*B*) XANES spectra of **1** (*a*), **2** (*b*), and **3** (*c*). (*C*) IR spectra of **3** treated with $^{12}CO$ (*d*) and a 1:1 mixture of $^{12}CO$ and $^{13}CO$ (*e*). The appearance of only four bands on adsorption of the mixture of CO isotopes indicates that the $^{12}CO$ bands at 2,202 and 2,188 $cm^{-1}$ correspond to two different chromium sites.

of THF per chromium center close to expected values (6 $C_4$/Cr, 1 THF/Cr). Diffuse reflectance UV-Vis (DRUV-Vis) spectra of **2** and **3** display similar absorption characteristics with a maximum at ∼700 nm along, with a shoulder at ∼470 nm (Fig. S1*B*), suggesting that the Cr environment is conserved during thermal treatment. Note that **1**, the molecular precursor, displays an absorption maximum at 400 nm in addition to the two features at 470 and 700 nm, consistent with its bluish-green color.

We performed XAS experiments on **1**, **2**, and **3** at the Cr–K edge to obtain more detailed information about the structure of the surface species. The X-ray near edge absorption spectroscopy (XANES) of **1**, **2**, and **3** are shown in Fig. 1*B*. The XANES for each species is at nearly identical edge energy, consistent with the conservation of the +3 oxidation state throughout the grafting and the thermal treatment process (22, 23). Note that the near-edge feature becomes more intense in the series of **1** to **2** to **3** and shifts from 6,006.0 (in **1**) to 6,007.5 eV (in **2** and **3**). Two pre-edge features are present in **1** at 5,989.5 and 5,991.8 eV. These features shift to 5,990.5 and 5,991.8 eV in **2**, albeit at lower intensities. The 5,990.5-eV pre-edge intensity decreases further in **3** with negligible contributions from higher-energy features. These changes in energy and position of the pre-edge features are probably associated with changes in the coordination number and local coordination symmetry of the chromium center that occurs during grafting and thermal treatment from consecutive loss of the two THF molecules and from exchanging siloxide ligands by the silica surface (23–26).

The extended X-ray absorption fine structures (EXAFS) of **1**, **2**, and **3** were analyzed, and the results are shown in Table 1. The fits include scattering paths from the three closest oxygen and silicon atoms from the siloxide ligands, and for **1** and **2**, additional paths of an oxygen atom and two nearby carbon atoms for each THF ligand. To simplify, averaged distances were used for Cr–O, Cr–C, and Cr–Si scattering paths, which gives statistically similar results to fits of **1** when using individual scattering paths and is consistent with the bond distances obtained from the X-ray structure (Fig. S2 and Table S1). With ∼1.96 Å, the Cr–O bonds for the three siloxide ligands in **2** and **3** are longer than the corresponding Cr–O bonds in **1**, but are consistent with reported Cr(III)–O bonds (27, 28). The fit of **3** is improved by including a fourth oxygen scattering path at longer Cr–O distances, likely accounting for the coordination of nearby siloxane bridges. The statistical quality of the fit was best for 0.4–0.5 oxygens per chromium, which suggests that 40–50% of the Cr(III) sites coordinate an additional oxygen, presumably an adjacent siloxane bridge. Taken together, the elemental analysis, mass balance, IR, UV-Vis, and XAS data are consistent with the formation of mononuclear Cr(III) sites in **3**, some of them presenting additional adjacent siloxane bridges.

Although the EXAFS results are consistent with the formation of **3**, they indicate that subtle structural variation of the Cr(III) sites may be present on the surface by presence or absence of coordinating siloxane bridges. Contacting **3** with excess CO (25 CO/Cr) results in two IR bands at 2,202 and 2,188 $cm^{-1}$ (Fig. 1*C*, spectrum d). To determine if these two $\nu_{CO}$ stretches are from two separate Cr sites or are the results of symmetric/asymmetric contributions, we contacted **3** with a 1:1 mixture of $^{13}CO$ and $^{12}CO$ (Fig. 1*C*, spectrum e). The presence of four bands, two assigned to $^{12}CO$ and two from the isotopically shifted $^{13}CO$ in the IR spectrum (vide infra, computational results), is consistent with the presence of two different Cr-sites.

The X-band EPR spectra of **1**, **2**, and **3** were recorded at 100 K (Fig. S3). All three spectra show a broad symmetric signal at

**Table 1. EXAFS fit parameters for 1, $[(\equiv SiO)Cr(OSi(O^tBu)_3)_2(THF)]$ 2, and $[(\equiv SiO)_3Cr]$ 3**

| Sample | Neighbor | *N** | *r* (Å)† | $\sigma^2$ (Å$^2$)‡ |
|---|---|---|---|---|
| **1**§ | O | 3 | 1.866(5) | 0.0049(9) |
| | O | 2 | 2.018(5) | 0.0049(9) |
| | C | 4 | 2.97(1) | 0.010(4) |
| | Si | 3 | 3.553(8) | 0.010(3) |
| **2**¶ | O | 3 | 1.95(3) | 0.013(3) |
| | O | 1 | 2.00(2) | 0.003(2) |
| | C | 2 | 3.02(2) | 0.003(2) |
| | Si | 3 | 3.2(1) | 0.05(3) |
| **3**¶ | O | 3 | 1.973(9) | 0.0027(8) |
| | O | 0.4 | 2.50(6) | 0.0027(8) |
| | Si | 3 | 3.21(2) | 0.009(2) |

Values without errors were fixed in the EXAFS fits.
*Number of neighbors.
†Distance between Cr and neighbor.
‡Debye–Waller factor.
§At 100 K in transmission mode.
¶At 100 K in fluorescence mode.

approximately $g = 4.9$ (width, ~600 G) and a dispersive signal at approximately $g = 2.0$ (peak-to-peak width, ~200 G), consistent with an axial g-tensor. The broad absorptive signal at lower magnetic field consists of two broad overlapping signals that are consistent with the presence of two different types of chromium environments in **3**.

**Ethylene Polymerization Activity.** The polymerization activity of **3** was monitored by IR spectroscopy at 70 °C at 325 mbar ethylene pressure. To avoid mass transfer limitations, Sylopol-948 was used as silica support due to its ability to fragment when a polymer is formed. Under these conditions, **3** has an initial ethylene polymerization activity of 15 kg polyethylene (PE) (mol Cr·h)$^{-1}$. HT-SEC of this polyethylene gives a number average molecular weight of $M_n$ = 33,600 g/mol and a weight average molecular weight of $M_w$ = 415,100 g/mol, corresponding to a dispersity $Đ = M_w/M_n$ = 12.3. The differential scanning calorimetry gives a broad melting temperature between 110 °C and 140 °C. Performing the polymerization in a fixed bed reactor at higher ethylene pressure (6 bar) at 70 °C gives 104 kg PE (mol Cr·h)$^{-1}$. The polymer produced by [(≡SiO)$_3$Cr] under high-pressure conditions has a similar dispersity ($Đ = M_w/M_n$ of 13.1) with a reduced molecular weight ($M_n$ = 8,000 g/mol, $M_w$ = 105,000 g/mol) and melts between 110 °C and 135 °C. The $^1$H NMR and $^{13}$C NMR spectra of the polymer under either low-pressure or high-pressure conditions are consistent with linear polyethylene with very low branching (<1 branches/1,000 C) (Fig. S4).

We titrated the number of active sites in **3** by poisoning experiments with 4-picoline. The polymerization activity of **3**, measured at 70 °C and 325 mbar of ethylene pressure, decreases linearly with an increasing amount of poison (Fig. S5*A*); activity ceases at 0.6 equivalents of poison per Cr, suggesting that ~60% of surface sites can initiate polymerization. These data are consistent with the CO studies and EPR spectroscopy discussed above that indicate the presence of at least two sites, only one of which is active.

The IR spectrum of **3** contacted with ethylene contains bands at 3,692, 3,643, and 3,605 cm$^{-1}$ in the OH region assigned to silanols interacting with the polymer (29) and silanols interacting with adjacent Cr(III) sites to form Si–(μ-OH)–Cr(III) species from the heterolytic cleavage of a C–H bond of ethylene across a Cr–O bond (8, 30–33). Consistent with this assignment, contacting **3** with $C_2D_4$ results in an isotopic shift of the band from 3,605 to 2,581 cm$^{-1}$ (Fig. S5*B*). Note that XANES before and after polymerization show identical edge energy, consistent with a conservation of oxidation state after catalysis.

**Density Functional Theory Calculations.** The experimental data presented above establish that two Cr(III) sites are present in **3**, 60% of which are active in ethylene polymerization, and that initiation involves heterolytic C–H activation of ethylene. To shed light on the possible structures of the active and inactive Cr(III) sites and on the polymerization mechanism (initiation, propagation, and termination), we carried out density functional theory (DFT) calculations using the hybrid functional B3LYP corrected for dispersion (D3).[†] Two types of Cr(III) sites were modeled as shown in Fig. 2*A*.[‡] We will focus the discussion on the high spin configuration of a $d^3$ Cr(III) ion because the quartet (S = 3/2) is 19.6 kcal/mol more stable than the doublet (S = 1/2) species for the model $\mathbf{3a_M}$. This cluster model was designed to account for the heterogeneity of the amorphous silica surface and the presence of mainly large (Si–O)$_n$ rings in the SiO network on silica ($n > 6$)

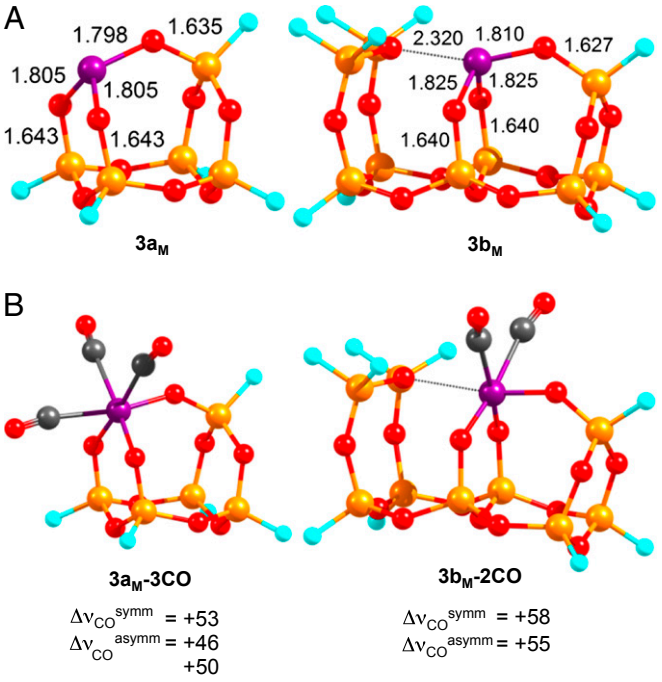


**Fig. 2.** (*A*) Cluster models for the silica-supported Cr(III) sites. (*B*) B3LYP/BS1 optimized structures of the tricarbonyl $\mathbf{3a_M}$ and the dicarbonyl $\mathbf{3b_M}$ and the corresponding CO frequency shifts. Color coding: purple, Cr; orange, Si; red, O; cyan, F; gray, C. Distances are given in Angstroms.

(36, 37): it presents a Cr(III) bonded to three siloxide oxygen atoms of a siloxane network making a cage which exposes two types of faces containing the Cr atom, one face with six-membered ring (Cr–O)(Si–O)$_2$ and two with eight-membered ring (Cr–O)(Si–O)$_3$ cycles. The silicon atoms of the clusters were saturated with fluorine atoms, which are good models for silica surfaces (14, 34, 38, 39). The calculated Cr–O bond distances in $\mathbf{3a_M}$ are ~1.80 Å, similar to the Cr–O distances in **1** and somewhat shorter than EXAFS distances in **3**.[§] Including one adjacent siloxane bridge in the cluster model as in $\mathbf{3b_M}$ shows that the siloxane bridge oxygen is 2.32 Å from Cr, slightly shorter than the distance obtained from EXAFS for an additional oxygen (2.50 Å). In all cases, natural bond orbital analysis of these models ($\mathbf{3a_M}$ and $\mathbf{3b_M}$) at B3LYP/TZVP on the B3LYP/BS1 geometries give a partial positive charge (natural population analysis charge of approximately +1.5) on the Cr(III) centers.

Up to three CO molecules can bind to $\mathbf{3a_M}$ with similar exoergic reaction energies for each additional coordinated CO (Table 2 and B3LYP/BS1 optimized structures in Fig. S6*A*). The tricarbonyl Cr(III) species presents calculated frequencies of $\nu_{CO}^{symm}$ and $\nu_{CO}^{asymm}$ that are blue shifted by +53 and +46/+50 cm$^{-1}$ with respect to free CO, respectively. Cluster $\mathbf{3b_M}$ can chemisorb only two CO molecules while maintaining the coordinated siloxane bridge at ~2.6 Å from the Cr(III) center and displays calculated CO vibrations shifted by +58 and +55 cm$^{-1}$ for the symmetric and antisymmetric modes, respectively.[¶] From a comparison of experimental and calculated $\nu_{CO}$ values, we propose that the blue-shifted signal at +59 cm$^{-1}$ comes from a dicarbonyl

[†]Calculations with the hybrid M06 functional gave very similar results.

[‡]We also explored the classical symmetric model with only six membered ring faces (34, 35) typically used for modeling tripodal species. Although this model binds CO and leads to similar calculated CO frequencies, siloxane cage opening occurs during C–H activation, probably due to ring strain in this model.

[§]Due to the simplicity and the flexibility of these models, only the most stable species are generated, which probably explains the small difference between calculated and observed Cr–O distances.

[¶]In view of the small calculated vibrational splitting (3 cm$^{-1}$) between the symmetric and asymmetric CO stretching frequencies, it is not expected to be able to distinguish the two bands and these of the expected isotopomers, so that the two experimentally observed bands must arise from two different sites.

**Table 2. Gibbs free energies of adsorption ($\Delta G_{ads}$, kcal/mol) and vibrational shifts of the CO moiety with respect to free CO ($cm^{-1}$) for mono-, di-, and tricarbonyl adducts**

| Cluster | 1 CO | 2 CO | 3 CO |
|---|---|---|---|
| **$3a_M$** | | | |
| $\Delta G_{ads}$ | −4.3 | −7.0 (−2.7) | −10.1 (−3.1) |
| $\Delta\nu_{CO}^{symm}$ | +61* | +56 | +53 |
| $\Delta\nu_{CO}^{asymm}$ | | +53 | +50/+46 |
| **$3b_M$** | | | |
| $\Delta G_{ads}$ | −4.8 | −8.7 (−3.9) | |
| $\Delta\nu_{CO}^{symm}$ | +60* | +58 | |
| $\Delta\nu_{CO}^{asymm}$ | | +55 | |

Gibbs free energies of adsorption are calculated according to the formula $\Delta G_{ads} = \Delta G_{cluster\text{-}nCO} - (\Delta G_{cluster} + n\Delta G_{CO})$. Values in parenthesis are calculated according to $\Delta G_{ads} = \Delta G_{cluster\text{-}nCO} - (\Delta G_{cluster\text{-}(n\text{-}1)CO} + \Delta G_{CO})$.
*Only one mode for the monocarbonyl adduct.

Cr(III) surface complex having an additional siloxane bridge (+58 $cm^{-1}$ for $\mathbf{3b_M}$), whereas that observed at +45 $cm^{-1}$ is attributed to a tricarbonyl Tris-siloxy Cr(III) surface complex (Fig. 2*B*). Finally, the calculated and observed blue-shifted values are consistent with the strongly cationic character of the Cr(III) centers, which induces electrostatic polarization of the CO molecular orbitals on coordination to a metal center (40, 41).

The reactivity of $\mathbf{3a_M}$ toward ethylene was explored as shown in Figs. 3 and 4 (B3LYP/BS1 optimized structures are shown in Figs. S6*B* and S7). During this study, we found that the doublet spin surface is much higher in energy than the quartet (at least 15 kcal/mol at the B3LYP-D3/BS1 level) from analysis of the whole Gibbs energy surface, indicating that polymerization takes place exclusively on the quartet surface.

Cluster $\mathbf{3a_M}$ can coordinate up to three ethylene molecules with favorable Gibbs reaction energies. When a single ethylene molecule is involved, the C–H bond activation on one of the Cr–O bonds of the six-member ring to form a Cr–vinyl species is associated with a transition state (**TS-4–5**) 32.9 kcal/mol above the separated reactants and corresponds to a σ-bond metathesis, as shown in Fig. 3*B* (42), where the O–H–$C_{vinyl}$ angle is 144° as expected for a σ-bond metathesis type proton transfer. The resulting Cr–vinyl complex **5** is 19.4 kcal/mol less stable than the separated reactants.

Including one additional coordinated molecule of ethylene results in a significant decrease in both the C–H activation transition state (+24.5 kcal/mol) and Gibbs reaction energy (+11.8 kcal/mol), without a significant change in the geometries of the transition state and the final Cr–vinyl surface species.[‖] However, when three molecules of ethylene are involved, the C–H activation TS could not be located. Alternative C–H bond activation on the eight-member ring of $\mathbf{3a_M}$ leads to similar energetics, indicating that tricoordinated Cr(III) sites can readily activate the C–H bond of ethylene. In contrast to $\mathbf{3a_M}$, cluster $\mathbf{3b_M}$ can absorb only one ethylene without losing the Cr–$O_{siloxane}$ interaction. This Cr–$O_{siloxane}$ bond distance was fixed at 2.6 Å because full optimization of ethylene coordinated $\mathbf{3b_M}$ led to loss of the Cr–$O_{siloxane}$ interaction, which seems improbable due to the rigidity of the silica support. Coordination of one ethylene molecule leads to a π-ethylene adduct 8.3 kcal/mol below separate reactants (close to the corresponding value of 9.0 kcal/mol for $\mathbf{3a_M}$) and an associated TS for C–H bond activation of ethylene of 40.1 kcal/mol,** which is higher than the corresponding step with $\mathbf{3a_M}$. Attempts to coordinate a second ethylene molecule to the Cr(III) center were unsuccessful. Given that the favored pathway for initiation with $\mathbf{3a_M}$ involves a dicoordinated surface complex (Fig. 3), this result suggests that Cr(III) sites coordinated to siloxane bridges, as in $\mathbf{3b_M}$, are inactive toward polymerization, whereas open sites, as in $\mathbf{3a_M}$, initiate polymerization. These data are consistent with the experimental results from EXAFS (40–50% of the sites coordinate an additional oxygen), CO adsorption (two sites), and the poisoning studies (60% active sites).

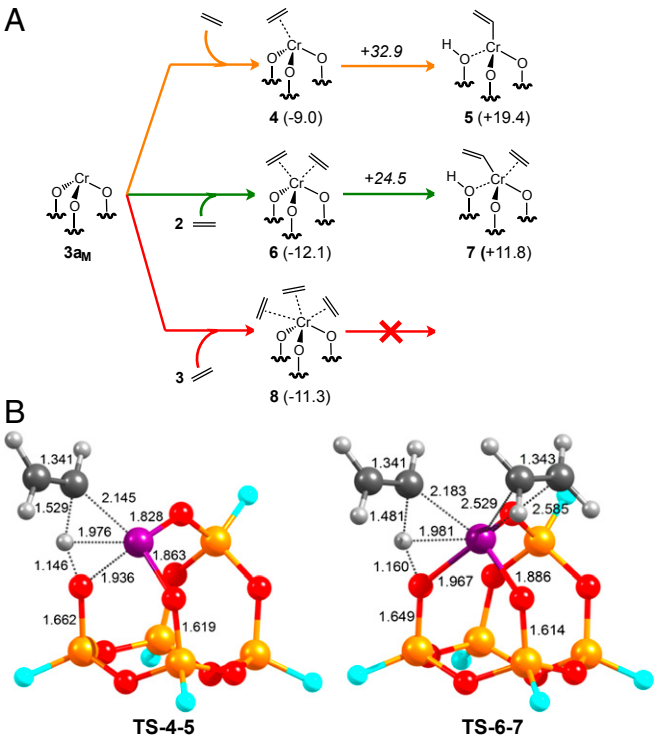


**Fig. 3.** (*A*) DFT study of the initiation mechanism of ethylene polymerization with $\mathbf{3a_M}$. Numbers in parentheses are Gibbs free energies of the corresponding intermediates and numbers in italic are Gibbs free energies of the corresponding transition states, normalized with respect to the system $\mathbf{3a_M}$ + 4 ethylene. All energies are in kcal/mol. (*B*) Transition state structures for the C-H bond activation in ethylene with $\mathbf{3a_M}$. Color coding: purple, Cr; orange, Si; red, O; cyan, F; gray, C; white, H. Distances are given in Angstroms.

We also explored alternative Cr–C bond formation pathways. One possibility is the oxidative cyclization of two ethylene molecules to form a chromacyclopentane species (43–45), whereas the other is a direct oxidative C–H bond activation to form a Cr–vinyl hydride, both of which are proposed initiation steps for the Phillips catalyst (13, 14, 46, 47). In both cases, we were unable to locate stable minima. These results, coupled with favorable apparent activation energies with model $\mathbf{3a_M}$, clearly support polymerization initiation by the heterolytic cleavage of the C–H bond on a Cr–O bond.

Fig. 4 shows the propagation and termination steps, together with the most favorable pathway for initiation, described above, representing the entire catalytic cycle for the production of an ethylene tetramer.

Insertion of ethylene into the Cr–vinyl species is highly exoergic (Gibbs reaction energies approximately –10 kcal/mol per ethylene) and is associated with a low energy transition state (9–14 kcal/mol with respect to the Cr–alkenyl–π complexes). Insertion of the first ethylene molecule into the Cr–vinyl **7** leads to a Cr–butenyl species **9** only +1.8 kcal/mol above separated

[‖]Note that these energy barriers values correspond to an upper limit because they were calculated using a model representing the most stable (and thereby less reactive) tricoordinated Cr-silicate.

**Although we found the correct imaginary frequency corresponding to the vibrational mode for the C–H activation step, we also found an additional imaginary component at ~22 $cm^{-1}$ due to the constrained structure of the TS. In view of this, the energy barrier of 40.1 kcal/mol should be understood as an indicative number of the height of the barrier.

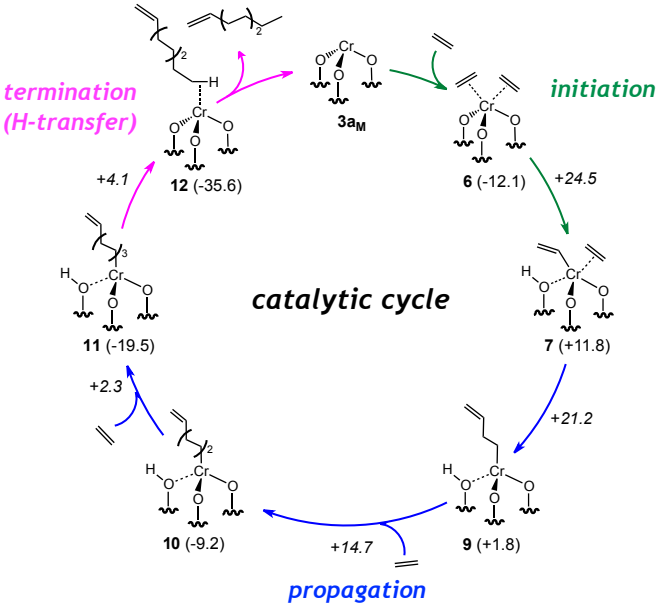


**Fig. 4.** Ethylene polymerization mechanism from DFT studies of **3a$_M$**. Numbers in parentheses are Gibbs free energies of the corresponding intermediates and numbers in italic are Gibbs free energies of the corresponding transition states, normalized with respect to the system **3a$_M$** + 4 ethylene. All energies are in kcal/mol.

reactants, indicating that the rate-determining step is associated with initiation and that propagation is fast (20, 48, 49).[††] Finally, termination by proton transfer takes place with a low energy barrier, leading to a highly stable intermediate **12**. The release of the oligomer from this intermediate is practically isoenergetic, regenerating the active species **3a$_M$**.

For the formation of the ethylene oligomer (polymer), we explored three different termination pathways from complex **10** (Fig. S8): proton transfer (microreverse of initiation), β-H transfer, and chain transfer to a monomer. Chain transfer to a coordinated monomer is the least favored termination pathway with an activation barrier with respect to **10** of +30.4 kcal/mol. Although the classical β-H transfer termination step has a lower energy barrier (+15.4 kcal/mol) than proton transfer (+23.8 kcal/mol), the release of the polymer, in this case an α,ω–diene, is thermodynamically unfavorable (reaction free energy with respect to **10** of +25.5 kcal/mol and formation of a highly unstable Cr hydride with respect to **3a$_M$**) and therefore associated with a higher reaction barrier. The preferred termination pathway is a proton transfer step corresponding to the microreverse of the C–H activation initiation step. The terminating proton transfer step from **9**, **10**, or **11** leads to intermediates that are about 15 kcal/mol more stable than the corresponding Cr–alkenyl species that is always associated with energy barriers 10–12 kcal/mol higher than insertion, consistent with chain growth over termination and the formation of high-molecular-weight polymers.

**Conclusion.** Cr(III) mononuclear sites on silica were prepared using a molecular approach. IR and EPR spectroscopies, as well as poisoning experiments, show that there are two different types of Cr(III) sites on the surface and that 60% of the Cr(III) sites can initiate ethylene polymerization. IR spectroscopy and DFT modeling indicate that the active sites are tricoordinated Cr(III) sites and that the first Cr–C bond forms through C–H activation on a Cr–O bond. Propagation on these sites by a Cossee–Arlman insertion mechanism and chain termination by the microreverse of the C–H activation step, a step associated with higher transition state energies than propagation, are consistent with favored polymerization over oligomerization and complete the catalytic cycle. In view of the amorphous character of the silica surface, it is expected that a distribution of tricoordinate Cr(III) sites are present, some being inactive. The reactivity of these sites in terms of initiation, propagation, and termination steps will vary, which explains the broad distribution of molecular weights in Cr-based silica-supported polymerization catalysts.

## Methods

Complete details of materials and methods are found in *SI Text*.

**Synthesis of Materials.** The synthesis of all materials are described in *SI Text*.

**Characterization Methods.** IR, UV/Vis, EPR and XAS methods are provided in *SI Text*.

**Polymerization Reactions.** The experimental methods used for polymerization reactions are given in *SI Text*.

**Computational Methods.** Details for the computational studies are provided in *SI Text*.

**ACKNOWLEDGMENTS.** G.S. and A.C.-V. thank the Swiss National Science Foundation (SNF 200021_137691/1 and Ambizione project PZ00P2_148059, respectively) for financial support.

[††]Note that the catalyst resting states hence corresponds to structures having Si–(μ-OH)–Cr(III) units, which is consistent with the observed red shifted OH.

1. McDaniel MP (2010) A review of the Phillips supported chromium catalyst and its commercial use for ethylene polymerization. *Advances in Catalysis*, eds Bruce CG, Helmut K (Academic Press, New York), Vol 53, pp 123–606.
2. Chen EY-X, Marks TJ (2000) Cocatalysts for metal-catalyzed olefin polymerization: Activators, activation processes, and structure-activity relationships. *Chem Rev* 100(4): 1391–1434.
3. Weckhuysen BM, Wachs IE, Schoonheydt RA (1996) Surface chemistry and spectroscopy of chromium in inorganic oxides. *Chem Rev* 96(8):3327–3350.
4. McDaniel MP, Martin SJ (1991) Poisoning studies on chromium/silica. 2. Carbon monoxide. *J Phys Chem* 95(8):3289–3293.
5. Bade OM, Blom R, Ystenes M (1998) Chromium allyls on silica: A study of structure and reactivity. *Organometallics* 17(12):2524–2533.
6. Amor Nait Ajjou J, Scott SL, Paquet V (1998) Synthesis and characterization of silica-stabilized chromium(IV) alkylidene complexes. *J Am Chem Soc* 120(2):415–416.
7. Beaudoin MC, et al. (2002) Silica-supported alkylidene complexes: Their preparation, characterization and reactivity, especially towards olefins. *J Mol Catal Chem* 190(1-2): 159–169.
8. Conley MP, et al. (2014) Polymerization of ethylene by silica-supported dinuclear Cr(III) sites through an initiation step involving C-H bond activation. *Angew Chem Int Ed Engl* 53(7):1872–1876.
9. MacAdams LA, Buffone GP, Incarvito CD, Rheingold AL, Theopold KH (2005) A chromium catalyst for the polymerization of ethylene as a homogeneous model for the phillips catalyst. *J Am Chem Soc* 127(4):1082–1083.
10. Theopold KH (1990) Organochromium(III) chemistry: A neglected oxidation state. *Acc Chem Res* 23(8):263–270.
11. Theopold KH (1998) Homogeneous chromium catalysts for olefin polymerization. *Eur J Inorg Chem* (1):15–24.
12. Beck DD, Lunsford JH (1981) The active site for ethylene polymerization over chromium supported on silica. *J Catal* 68(1):121–131.
13. Espelid O, Borve KJ (2000) Theoretical models of ethylene polymerization over a mononuclear chromium(II)/silica site. *J Catal* 195(1):125–139.
14. Espelid O, Borve KJ (2002) Molecular-level insight into Cr/silica Phillips-type catalysts: Polymerization-active mononuclear chromium sites. *J Catal* 205(2):366–374.
15. McDaniel MP (1981) The state of Cr(VI) on the Cr/Silica polymerization catalyst. *J Catal* 67(1):71–76.
16. McDaniel MP (1982) The state of Cr(VI) on the Phillips polymerization catalyst: II. The reaction between silica and CrO2Cl2. *J Catal* 76(1):17–28.
17. McDaniel MP (1982) The state of Cr(VI) on the Phillips polymerization catalyst: III. The reaction between CrO3/silica and HCl. *J Catal* 76(1):29–36.
18. McDaniel MP (1982) The state of Cr(VI) on the Phillips polymerization catalyst: IV. Saturation coverage. *J Catal* 76(1):37–47.
19. Ciborska A, Chojnacki J, Wojnowski W (2007) Bis(tetrahydrofuran-[kappa]O)tris(tri-tert-butoxysiloxy)chromium(III). *Acta Crystallogr Sect E Struct Rep Online* 63(4): m1103–m1104.
20. Grubbs RH, Coates GW (1996) α-Agostic interactions and olefin insertion in metallocene polymerization catalysts. *Acc Chem Res* 29(2):85–93.

21. Coates GW, Hustad PD, Reinartz S (2002) Catalysts for the living insertion polymerization of alkenes: Access to new polyolefin architectures using Ziegler-Natta chemistry. *Angew Chem Int Ed Engl* 41(13):2237–2257.
22. Berry AJ, O'Neill HSC (2004) A XANES determination of the oxidation state of chromium silicate glasses. *Am Mineral* 89(5-6):790–798.
23. DuBois JL, et al. (2000) A systematic K-edge X-ray absorption spectroscopic study of Cu(III) sites. *J Am Chem Soc* 122(24):5775–5787.
24. Kau LS, Spira-Solomon DJ, Penner-Hahn JE, Hodgson KO, Solomon EI (1987) X-ray absorption edge determination of the oxidation state and coordination number of copper. Application to the type 3 site in Rhus vernicifera laccase and its reaction with oxygen. *J Am Chem Soc* 109(21):6433–6442.
25. Westre TE, et al. (1997) A multiplet analysis of Fe K-Edge 1s → 3d pre-edge features of iron complexes. *J Am Chem Soc* 119(27):6297–6314.
26. George SD, Brant P, Solomon EI (2005) Metal and ligand K-edge XAS of organotitanium complexes: Metal 4p and 3d contributions to pre-edge intensity and their contributions to bonding. *J Am Chem Soc* 127(2):667–674.
27. Thomas BG, Morris ML, Hilderbrandt RL (1978) Structure of tris(1,1,1,5,5,5-hexafluoro-2,4-pentanedionato)chromium(III) determined by gas-phase electron diffraction. *Inorg Chem* 17(10):2901–2905.
28. Levina A, Foran GJ, Pattison DI, Lay PA (2004) X-ray absorption spectroscopic and electrochemical studies of tris(catecholato(2-))chromate(V/IV/III) complexes. *Angew Chem Int Ed Engl* 43(4):462–465.
29. van der Meer J, et al. (2010) Mechanism of metal oxide nanoparticle loading in SBA-15 by the double solvent technique. *J Phys Chem C* 114(8):3507–3515.
30. Cappus D, et al. (1993) Hydroxyl groups on oxide surfaces: NiO(100), NiO(111) and Cr2O3(111). *Chem Phys* 177(2):533–546.
31. Henderson MA, Chambers SA (2000) HREELS, TPD and XPS study of the interaction of water with the α-Cr2O3(001) surface. *Surf Sci* 449(1-3):135–150.
32. Hadjiivanov K, Penkova A, Kefirov R, Dzwigaj S, Che M (2009) Influence of dealumination and treatments on the chromium speciation in zeolite CrBEA. *Microporous Mesoporous Mater* 124(1-3):59–69.
33. Dzwigaj S, Shishido T (2008) State of chromium in CrSiBEA zeolite prepared by the two-step postsynthesis method: XRD, FTIR, UV-Vis, EPR, TPR, and XAS studies. *J Phys Chem C* 112(15):5803–5809.
34. Espelid O, Borve KJ (2001) Theoretical analysis of d-d transitions for the reduced Cr/silica system. *Catal Lett* 75(1-2):49–54.
35. Espelid O, Borve KJ (2002) Theoretical analysis of CO adsorption on the reduced Cr/silica system. *J Catal* 205(1):177–190.
36. Stallons JM, Iglesia E (2001) Simulations of the structure and properties of amorphous silica surfaces. *Chem Eng Sci* 56(14):4205–4216.
37. Zhuravlev LT (2000) The surface chemistry of amorphous silica. Zhuravlev model. *Colloid Surface A* 173(1-3):1–38.
38. Damin A, et al. (2009) Modeling CO and N2 adsorption at Cr surface species of Phillips catalyst by hybrid density functionals: Effect of Hartree-Fock exchange percentage. *J Phys Chem A* 113(52):14261–14269.
39. Espelid O, Borve KJ (2002) Molecular-level insight into Cr/silica Phillips-Type catalysts: Polymerization-active dinuclear chromium sites. *J Catal* 206(2):331–338.
40. Lupinetti AJ, Strauss SH, Frenking G (2001) Nonclassical metal carbonyls. *Progress in Inorganic Chemistry*, ed Karlin KD (John Wiley & Sons, Inc., Hoboken, NJ), Vol 49, pp 1–112.
41. Willner H, Aubke F (1997) Homoleptic metal carbonyl cations of the electron-rich metals: Their generation in superacid media together with their spectroscopic and structural characterization. *Angew Chem Int Ed Engl* 36(22):2403–2425.
42. Balcells D, Clot E, Eisenstein O (2010) C-H bond activation in transition metal species from a computational perspective. *Chem Rev* 110(2):749–823.
43. Agapie T, Schofer SJ, Labinger JA, Bercaw JE (2004) Mechanistic studies of the ethylene trimerization reaction with chromium-diphosphine catalysts: Experimental evidence for a mechanism involving metallacyclic intermediates. *J Am Chem Soc* 126(5):1304–1305.
44. Agapie T, Labinger JA, Bercaw JE (2007) Mechanistic studies of olefin and alkyne trimerization with chromium catalysts: Deuterium labeling and studies of regiochemistry using a model chromacyclopentane complex. *J Am Chem Soc* 129(46): 14281–14295.
45. Do LH, Labinger JA, Bercaw JE (2012) Mechanistic studies of ethylene and α-olefin co-oligomerization catalyzed by chromium-PNP complexes. *Organometallics* 31(14): 5143–5149.
46. Zhong L, et al. (2012) Active site transformation during the induction period of ethylene polymerization over the Phillips CrOx/SiO2 catalyst. *Chemcatchem* 4(6): 872–881.
47. Schmid R, Ziegler T (2000) Ethylene-polymerization by surface supported Cr(IV) species: Possible reaction mechanisms revisited by theoretical calculations. *Can J Chem* 78(2):265–269.
48. Burger BJ, Thompson ME, Cotter WD, Bercaw JE (1990) Ethylene insertion and beta-hydrogen elimination for permethylscandocene alkyl complexes: A study of the chain propagation and termination steps in Ziegler-Natta polymerization of ethylene. *J Am Chem Soc* 112(4):1566–1577.
49. Rappé AK, Skiff WM, Casewit CJ (2000) Modeling metal-catalyzed olefin polymerization. *Chem Rev* 100(4):1435–1456.